

# Inhomogeneous BCS-BEC crossover for trapped cold atoms in optical lattices

A. Amaricci,<sup>1</sup> A. Privitera,<sup>1</sup> and M. Capone<sup>1</sup>

<sup>1</sup>*Democritos National Simulation Center, Consiglio Nazionale delle Ricerche, Istituto Officina dei Materiali (IOM) and Scuola Internazionale Superiore di Studi Avanzati (SISSA), Via Bonomea 265, 34136 Trieste, Italy*

The BCS-BEC crossover in a lattice is a powerful paradigm to understand how a superconductor deviates from the Bardeen-Cooper-Schrieffer physics as the attractive interaction increases. Optical lattices loaded with binary mixtures of cold atoms allow to address it experimentally in a clean and controlled way. We show that, however, the possibility to study this phenomenon in actual cold-atoms experiments is limited by the effect of the trapping potential. Real-space Dynamical Mean-Field Theory calculations show indeed that interactions and the confining potential conspire to pack the fermions in the center of the trap, which approaches a band insulator when the attraction become sizeable. We show how this physics reflects in several observables, and we propose an alternative strategy to disentangle the effect of the harmonic potential and measure the intrinsic properties resulting from the interaction strength.

PACS numbers: 71.10.Fd, 03.75.Ss, 05.30.Fk, 67.85.Lm

The experimental advances in handling and probing cold atoms in optical lattices open a new path towards the understanding of popular condensed-matter lattice models[1]. While the repulsive Fermi-Hubbard model and its Mott insulating phase[2, 3] are the first natural goal because of their relation with high-temperature superconductivity, the experimental realization[4] of the attractive Fermi-Hubbard model (AHM) is an equally sensible target. The quantum simulation of the AHM has at least a twofold motivation: besides its direct significance as an idealized description of actual superconductors, it has been proposed as a simpler path to investigate the repulsive model[5] exploiting an exact mapping between the two models.

At low temperature the AHM describes a superfluid (SF) state, whose properties evolve continuously from a weak-coupling Bardeen-Cooper Schrieffer (BCS) regime to a Bose-Einstein condensation (BEC) of preformed pairs as the attractive interaction is increased. The lattice counterpart of the BCS-BEC crossover[6] has been proposed as an effective description of high-temperature superconductors, and it displays significant differences with the crossover of dilute Fermi gases[7] including a pronounced maximum for intermediate pairing strength of the critical temperature, which vanishes as  $1/U$  for large attraction and a characteristic dependence on the lattice density, *i.e.* the number of fermions ( $N$ ) per lattice site  $n = N/N_s$ .

The description of the lattice BCS-BEC crossover requires non-perturbative approaches, among which Dynamical mean-field theory (DMFT)[8] can be particularly useful, as it correctly reproduces the exact solution both in the weak- and in the strong-coupling limit[9, 10] as well as the evolution of the normal state from which superfluidity establishes[11, 12]. DMFT also recovers the familiar BCS-BEC crossover for a Fermi gas in the dilute limit[13, 14].

However, DMFT enforces translational symmetry, which is clearly broken by the harmonic potential which traps the fermions in cold-atoms experiments. This requires to use an extension of DMFT, the real-space DMFT in order to take into account the inhomogeneity of the system and to investigate the effect of the trap on the BCS-BEC crossover. The same method, with a different impurity solver (see below), has been used in Ref.15 to identify a coexistence of SF and density-wave. While our focus is different, we mention that we did not observe a tendency to density ordering, in agreement with the Quantum Monte Carlo results of Ref.16.

Our zero-temperature calculations show that increasing the attraction strength leads to a compression of the cloud, with a central region populated by two fermions of opposite spin per lattice site, as in a band insulating state, leading to a packed cloud with reduced pairing amplitude. This collapse as a function of the interaction prevents us from reaching the actual BEC regime of the AHM, where local pairs are formed, but they do not coalesce in the same region of space. Indeed, the anomalous expansion of the cloud observed in experiments[4] does not overcome this limitation, as it is essentially due to adiabatic heating[17], an effect which introduces a further obstacle to the observation of the BCS-BEC crossover by effectively increasing the temperature at fixed entropy. We characterize the hidden crossover with observables which are accessible in the current cold-atoms experiments, like the momentum distribution function and the single-particle spectral functions. In addition, we propose a simple way to reduce the impact of the cloud compression and unveil the “homogeneous” BCS-BEC crossover compensating the effect of the inhomogeneous potential.

In all the calculations we consider an attractive Fermi-Hubbard model on a two-dimensional square optical lattice and placed in an external harmonic potential. The

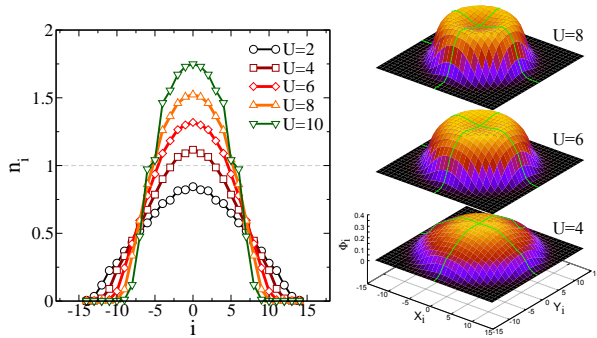


Figure 1: (Color online) Left panel: local density  $n_i$  profiles along the x-axis of the lattice ( $y_i = 0$ ) for  $N = 200$  fermions,  $V_0 = 0.03$ , and increasing attraction  $U$ . Data are for a lattice of  $N_s = 29 \times 29$  sites. Right panel: evolution of the corresponding superfluid amplitude  $\phi_i$  surface and profiles for  $U = 4$  (bottom),  $U = 6$  (center) and  $U = 8$  (top).

Hamiltonian reads:

$$\mathcal{H} = -t \sum_{\langle i,j \rangle \sigma} c_{i\sigma}^\dagger c_{j\sigma} - U \sum_i n_{i\uparrow} n_{i\downarrow} + \sum_{i\sigma} V_i n_{i\sigma} \quad (1)$$

where  $t$  is the hopping parameter between neighboring sites, which we set as the energy unit. The second term describes the local attractive interaction between fermions. Finally, the last term  $V_i = \frac{V_0}{2} (r_i/a)^2$  is the harmonic trapping potential, that we assumed with spherical symmetry,  $a$  is the the lattice spacing and  $r_i$  is the distance of the site  $i$  from the trap center.

We solve Eq. (1) on a lattice of  $N_s$  sites, using real-space DMFT[18–20], an extension of DMFT[8] introduced to treat inhomogeneous system. The key approximation is to assume a local, albeit site-dependent, self-energy matrix  $\hat{\Sigma}_{ij} = \delta_{ij} \hat{\Sigma}_i$ . Each local self-energy is obtained by solving an impurity problem defined by a site-dependent bath  $\hat{G}_0^{-1}$ , which is determined self-consistently by requiring that the single-particle Green function  $\hat{G}_i$  of each local impurity model coincides with the corresponding diagonal term of  $\hat{G}^{-1} = \hat{G}_0^{-1} - \hat{\Sigma}$ , where  $(\hat{G}_0^{-1})_{ij} = \delta_{ij}[\omega^+ - (V_i - \mu)] - \hat{t}_{ij}$  is the non-interacting Green's function and  $\hat{t}_{ij}$  is the lattice tight-binding matrix. In order to deal with superfluid phase, we recast the method in the Nambu spinor formalism[15], introducing anomalous (pair) Green's functions and self-energy components  $\hat{F}_i$  and  $\hat{S}_i$ , respectively.

The number of independent impurity models is reduced by the lattice  $C_{4v}$  symmetry. The solution of the impurity problems is obtained using the Iterated Perturbation Theory solver[8, 21], extended to deal with superconducting formalism[9]. This method provides an accurate and computationally cheap solver which gives direct access to dynamical properties including the local spectral functions  $\rho_i(\omega) = -\text{Im}G_i(\omega)/\pi$  at the site  $i$  and hence to the local spectral gap  $E_i^g$ . This information can be experimentally accessed by a spectroscopic

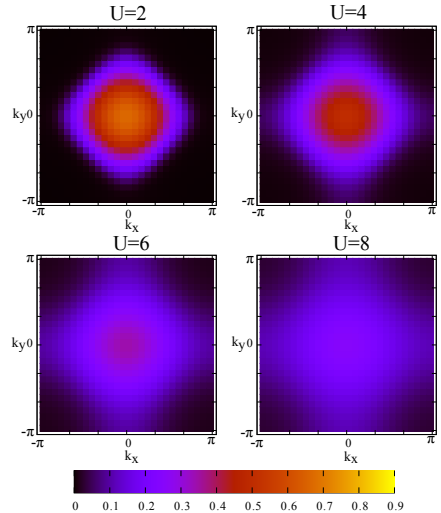


Figure 2: (Color online) Evolution of the momentum distribution  $n_k$  as a function of the increasing attraction  $U$ . Data are obtained for a lattice of  $N_s = 29 \times 29$  sites. The other model parameters as in Fig. 1

technique able to probe the local value of the gap (see e.g. [22] for a cold-atom analogue of the scanning tunneling microscopy used in condensed matter). We shall compare our calculations with local-density approximation (LDA) results where the local observables on each site are those of a homogeneous system with chemical potential  $\mu_i = \mu - V_i$ .

We briefly recall the main properties of the SF phase for the homogeneous Hubbard model. The modulus of the superfluid order parameter  $\phi = 1/N_s \sum_i \phi_i = 1/N_s \sum_i \langle c_{i\uparrow} c_{i\downarrow} \rangle$  and the spectral gap  $E^g$  monotonically increases as a function of  $U$ , while the critical temperature decreases for intermediate and large  $U$  because the large pairing strength locks the fermions in on-site pairs, which are strongly bound, but they move only through virtual processes of order  $t^2/U$  (a small number if  $U \gg t$ ), making it harder and harder to establish phase coherence over the whole system, a necessary condition for a SF state. As a consequence, the critical temperature in this regime is controlled by the superfluid stiffness, in turn proportional to  $t^2/U$  and decreases rapidly, as opposed to the weak-coupling regime, where the standard result  $T_c \propto \phi$  is recovered. The BEC side of the crossover is characterized also by a kinetic-energy gain which stabilizes the SF state, in contrast with the BCS theory, where a potential-energy gain leads to the SF[10]. Pairing without phase coherence results, in strong-coupling, to a normal state with a pseudogap in the spectrum. The lattice periodicity also introduces a peculiar dependence on the density.  $\phi$  is non monotonic as a function of the lattice filling, with a maximum at half-filling  $n = 1$  and a vanishing value for empty and completely filled lattice.

In Fig. 1 we show the evolution of the density profile  $n_i = \sum_{\sigma} \langle c_{i\sigma}^\dagger c_{i\sigma} \rangle$  and of the local pairing amplitude  $\phi_i$

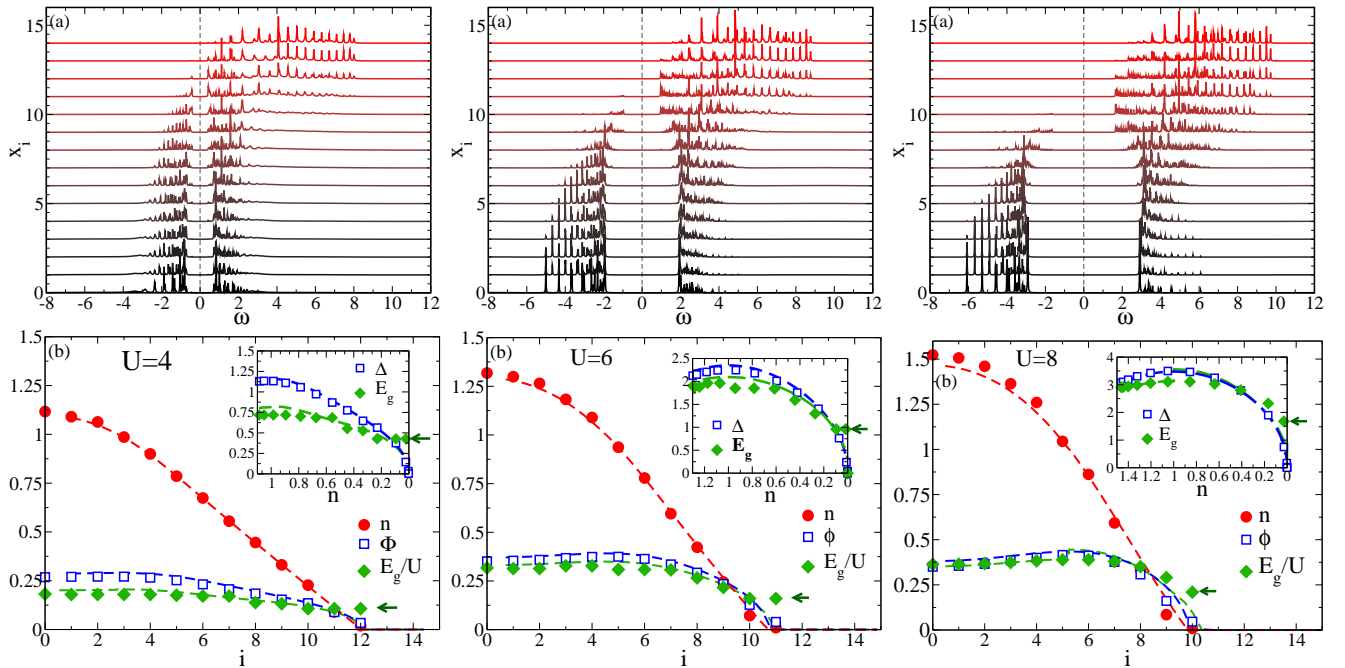


Figure 3: (Color online) Spectral functions (a) and energy gap (b) evolution of the trapped system along the  $y_i = 0$  axis for  $U = 4$  (left),  $U = 6$  (center) and  $U = 8$  (right). Other parameters are:  $V_0 = 0.03$ ,  $N = 200$  and system size is  $N_s = 29 \times 29$  sites. The top panels report the distribution of the density  $n_i$ , the amplitude  $\phi_i$  and the gap  $E_i^g$ . The insets show the behavior of the order parameter  $\Delta_i$  and gap  $E_i^g$  as a function of the density. The arrows indicate the large discontinuity at the border of the cloud.

for increasing  $U$  along the  $y_i = 0$  for  $N = 200$  fermions on a lattice of  $N_s = 29 \times 29$  sites. As pointed out in Ref. 15, by defining a typical radius  $r_c$  such that  $\frac{V_0}{2}(r_c/a)^2 = t$  and rescaling the density profiles in units of  $r_c$ , the results for fixed  $\mu$  and increasing  $r_c$ , *i.e.* increasing  $N$  and decreasing  $V_0$ , nicely collapse on the same curve. Thus our results are directly relevant for current experiments in ultracold gases as they can be easily extrapolated to actual system size and number of particles.

The density profiles for moderate and large  $U$  show that the confining potential and the interaction concur in pushing the fermions towards the trap center and in squeezing the cloud size. This effect is clearly triggered by the presence of the harmonic potential which favors a higher occupation of the central region. In the presence of an attractive interaction, this tendency is further enhanced by the energy gain associated to doubly occupied sites. This leads, as the interaction grows, to a packing of the central region, in which most of the fermions are confined, which approaches a local density of  $n = 2$  (as for a band insulator), giving rise to a more compact cloud with sharper boundaries with respect to a repulsive case, in which the interaction spreads the fermions in space.

The local superfluid amplitude  $\phi_i$ , shown in the right side of Fig. 1, has a non-trivial evolution. For weak interaction  $\phi_i$  is maximum at the trap center, and decreases monotonously moving towards the edges of the conden-

sate. Increasing the interaction, for  $U = 6t$  the maximum at the center turns into a minimum while a shallow maximum develops at a distance from the center. By further increasing the interaction the maximum moves at larger distances, while the whole pairing profile decreases.

This behavior can be traced back -in a LDA scheme- to nonmonotonic behavior as a function of filling, which is symmetric around a maximum at half-filling. Increasing the local density beyond half-filling is therefore expected to lead to a decrease of  $\phi$ . For our number of electrons, which would correspond to a density  $n \simeq 0.238$  in a homogeneous system, at weak coupling the cloud compression due to trap and interaction is not strong enough to raise the local density  $n_0$  in the trap center above 1. In this case  $\phi_i$  is maximum in the trap center and decreases monotonously as a function of the distance from the trap center. At large  $U$  instead the cloud compression becomes strong enough to have  $n_0 > 1$  and, although the attraction is larger, the order parameter in the trap center is suppressed, and the SF order amplitude acquires a ring shape, with a maximum amplitude around the line where the local density crosses  $n_i = 1$ .

It is important to notice that, besides the peculiar spatial pattern of the pairing amplitude, the collapse of the fermionic cloud significantly reduces the whole superfluid properties with respect to a homogeneous system with the same interaction strength and number of fermions.

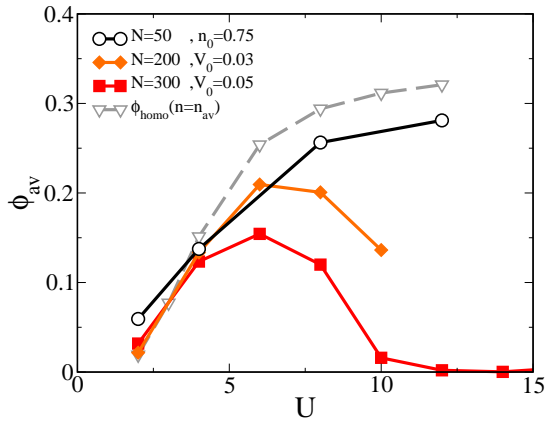


Figure 4: (Color online) Superfluid amplitude  $\phi$  as a function of interaction  $U$ . Data are obtained using different protocols for the BCS-BEC crossover using a total number of particles  $N = 50$  (open circles)  $N = 200$  (filled triangles) and  $N = 300$  (filled squares) respectively fixing the density at the center to  $n_0 = 0.75$  or fixing the harmonic potential strength to  $V_0 = 0.03$  (triangles) and  $V_0 = 0.05$  (squares). Dashed line indicates the homogeneous solution  $\phi_{homo}$  at average density  $n_{av}$  for  $N = 50$  and  $n_0 = 0.75$ .

This is associated to the proliferation of empty and doubly occupied sites, configurations that share a vanishing pairing amplitude. Therefore the BCS-BEC crossover we would observe in a homogeneous system is hidden by this effect, which starts already for intermediate coupling.

The same crossover is reflected in the momentum distribution function  $n_k$  (see Fig. 2), which is easily accessible in time-of-flight measurements. Once again, the DMFT results spotlight a rapid evolution from a BCS regime, characterized by ballistic expansion of the fermions to an intermediate coupling in which most fermions are gathered in the center of the trap. The evolution of  $n_k$  as a function of  $U$  shows indeed how the remnant Fermi surface abruptly turns into a broad distribution, characteristic of localized incoherent particles.

We now discuss how this physics reflects in the single-particle spectra and in the momentum distribution function, before proposing a simple way to unveil the properties of the homogeneous crossover. In the top panels of Fig. 3 we show the evolution of the local single-particle spectral function  $\rho_i(\omega) = -1/\pi \text{Im}G_i(\omega^+)$  along a cut parallel to the x-axis from the trap center (bottom) to the edge (top) for three different values of  $U$ . Notice that the discrete nature of the spectral function is a genuine feature due to the finite lattice and the trapping potential and it does not result from the DMFT treatment or from our solution method.

The main changes in the spectral functions as we move from the center to the boundary of the trap are associated to the change in local density. Interestingly, the energy gap  $E_i^g$  appears more uniform than the whole spectral

function. In the lower panels of Fig. 3 we report  $E_i^g$  as a function of the lattice position, together with the corresponding values of  $n_i, \phi_i$ . For the sake of comparison,  $E_i^g$  is divided by  $U$ , so that it can be more closely compared with  $\phi_i$  (in the BCS regime  $E^g = U\phi$ ). LDA results are shown for comparison as dashed lines.

Even if the global change in the curves going from the center to the edge of the trap may suggest that the DMFT results are well reproduced by LDA, significant deviations appear in the most delicate border region (notice that the center of the trap hosts an essentially trivial state). Interestingly, the spectral gap shows the most significant deviations with respect to LDA.  $E_i^g$  remains indeed essentially uniform in space also in the proximity of the cloud edge, while  $\phi_i$  vanishes as predicted by LDA. This leads to a strong deviation from the BCS proportionality between the two observables. As a matter of fact, the boundary of the cloud behaves like a phase-disordered superconductor with a finite spectral gap which is not accompanied by an actual SF order parameter. A similar behavior is indeed observed in Ref. 23 in the context of chemically disordered superconductors.

Our DMFT solution of the AHM in a trapping potential prompts that, in order to reveal the full BCS-BEC crossover, a more careful ad-hoc protocol has to be used. In particular one needs to compensate the cloud compression due to the increased interaction and keep the density as uniform as possible and, most importantly, independent on  $U$ . The simplest knob we can use to this end is the strength of the trapping potential. When  $U$  increases, we can decrease  $V_0$  and compensate for the cloud compression. As a matter of fact, it turns out that a suitable change of  $V_0$  is sufficient to reproduce an essentially constant density pattern for a wide range of  $U$ . This compensation protocol avoids the collapse of the cloud and allows for a sensible comparison between different values of  $U$ .

In Fig. 4 we show the performance of this compensation protocol. We perform calculations for different values of  $U$ , choosing  $V_0$  in order to keep constant the density at the trap center  $n_0 = 0.75$ . In order to compare results obtained with different protocols and potential widths, we estimated the average value of observables by averaging over sites with local occupancy larger than a small threshold  $n_i > 0.001$ . Even with this simple requirement, also the average density in the cloud is essentially constant as  $U$  goes from 2 to 12. The success of this choice in revealing the properties of the BCS-BEC crossover is testified by the main panel of Fig. 4, where the average pairing amplitude  $\phi_{av}$  for both the straightforward calculations at fixed  $V_0$  and for fixed  $n_0$ . It is apparent that calculations at fixed  $V_0$  fail in describing the monotonic increase of  $\phi_{av}$  as the interaction grows, and they decrease after a maximum which depends on  $V_0$ . On the other hand, the compensated protocol is perfectly able to reproduce the qualitative trend of the homogeneous

crossover.

We have shown that the detection of the BCS-BEC crossover in the AHM by means of cold-atoms in optical lattices is not straightforward. Using the same trapping potential and increasing the value of the attractive potential  $U$ , we are not able to reach a proper BEC regime because the fermionic cloud collapses into a packed “band-insulating” state with two fermions per site. This physics is reflected in the most important observables, including the local spectral function, the local energy gap and the momentum distribution function. Interestingly, the energy gap is more homogeneous than the superfluid order parameter and significantly deviates from local-density approximation.

The limitations introduced by the trapping potential can be overcome by tuning the strength of the potential in order to keep the density at the center of the trap independent on the value of  $U$ . This simple choice leads to an essentially fixed density pattern which allows to recover the main features of the lattice BCS-BEC crossover. A similar protocol should also be used to study more complex situations with population[24] and/or mass[25, 26] imbalance between the two fermionic species in order to reveal new exotic phases such as Sarma states and FFLO superfluidity.

This work is financed by ERC/FP7 through the Starting Independent Grant “SUPERBAD”, Grant Agreement No. 240524. We also acknowledge support of LEM-SUPER project (Grant Agreement no. 283214)

- 
- [1] I. Bloch, J. Dalibard, and S. Nascimbene, *Nat Phys* **8**, 267 (2012).
- [2] R. Jordens, N. Strohmaier, K. Gunter, H. Moritz, and T. Esslinger, *Nature* **455**, 204 (2008).
- [3] R. Jordens, L. Tarruell, D. Greif, T. Uehlinger, N. Strohmaier, H. Moritz, T. Esslinger, L. De Leo, C. Kollath, A. Georges, et al., *Phys. Rev. Lett.* **104**, 180401 (2010).
- [4] L. Hackermüller, U. Schneider, M. Moreno-Cardoner, T. Kitagawa, T. Best, S. Will, E. Demler, E. Altman, I. Bloch, and B. Paredes, *Science* **327**, 1621 (2010).
- [5] A. F. Ho, M. A. Cazalilla, and T. Giamarchi, *Phys. Rev. A* **79**, 033620 (2009).
- [6] P. Nozieres and S. Schmitt-Rink, *J. Low Temp. Phys.* **59**, 195 (1985).
- [7] W. Zwerger, *The BCS-BEC Crossover and the Unitary Fermi Gas* (Springer-Verlag Berlin Heidelberg, 2012).
- [8] A. Georges, G. Kotliar, W. Krauth, and M. J. Rozenberg, *Rev. Mod. Phys.* **68**, 13 (1996).
- [9] A. Garg, H. Krishnamurthy, and M. Randeria, *Phys. Rev. B* **72**, 024517 (2005).
- [10] A. Toschi, P. Barone, M. Capone, and C. Castellani, *New J. Phys.* **7** (2005).
- [11] M. Keller, W. Metzner, and U. Schollwöck, *Phys. Rev. Lett.* **86**, 4612 (2001).
- [12] M. Capone, C. Castellani, and M. Grilli, *Phys. Rev. Lett.* **88**, 126403 (2002).
- [13] A. Privitera, M. Capone, and C. Castellani, *Phys. Rev. B* **81**, 014523 (2010).
- [14] A. Privitera and M. Capone, *Phys. Rev. A* **85**, 013640 (2012).
- [15] A. Koga, T. Higashiyama, K. Inaba, S. Suga, and N. Kawakami, *Phys. Rev. A* **79**, 013607 (2009).
- [16] E. Assmann, S. Chiesa, G. G. Batrouni, H. G. Evertz, and R. T. Scalettar, *Phys. Rev. B* **85**, 014509 (2012).
- [17] B. Schmidt, M. R. Bakhtiari, I. Titvinidze, U. Schneider, M. Snoek, and W. Hofstetter, *Phys. Rev. Lett.* **110**, 075302 (2013).
- [18] R. W. Helmes, T. A. Costi, and A. Rosch, *Phys. Rev. Lett.* **100**, 056403 (2008).
- [19] E. C. Andrade, E. Miranda, and V. Dobrosavljević, *Phys. Rev. Lett.* **102**, 206403 (2009).
- [20] E. Miranda and V. Dobrosavljević, *Dynamical mean-field theories of correlation and disorder* (Oxford University Press, 2012).
- [21] H. Kajueter, G. Kotliar, and G. Moeller, *Phys. Rev. B* **53**, 16214 (1996).
- [22] T. Gericke, P. Wurtz, D. Reitz, T. Langen, and H. Ott, *Nat. Phys.* **4**, 949 (2008).
- [23] B. Sacepe, T. Dubouchet, C. Chapelier, M. Sanquer, M. Ovadia, D. Shahar, M. Feigelman, and L. Ioffe, *Nat. Phys.* **7**, 239 (2011).
- [24] T.-L. Dao, M. Ferrero, A. Georges, M. Capone, and O. Parcollet, *Phys. Rev. Lett.* **101**, 236405 (2008).
- [25] T.-L. Dao, A. Georges, and M. Capone, *Phys. Rev. B* **76**, 104517 (2007).
- [26] T.-L. Dao, M. Ferrero, P. S. Cornaglia, and M. Capone, *Phys. Rev. A* **85**, 013606 (2012).